Optimizing electrical contacts on individual p-i-n GaAs nanowires by site-specific focused ion beam processing

Citation for the original published paper (version of record):
Holmér, J., Zeng, L., Olsson, E. (2026). Optimizing electrical contacts on individual p-i-n GaAs nanowires by site-specific focused ion
beam processing. Nanotechnology, 37(36). http://dx.doi.org/10.1088/1361-6528/ae9d24

Optimizing electrical contacts on individual p–i–n GaAs nanowires by site-specific focused ion beam processing

Nanotechnology

Check for updates

OPEN ACCESS

RECEIVED
18 February 2026

REVISED
21 May 2026

ACCEPTED FOR PUBLICATION
23 August 2026

PUBLISHED
4 September 2026

PAPER

Optimizing electrical contacts on individual p–i–n GaAs nanowires by site-specific focused ion beam processing

Jonatan Holmér, Lunjie Zeng* and Eva Olsson*

Department of Physics and Astronomy, Chalmers University of Technology, Gothenburg 41296, Sweden
* Authors to whom any correspondence should be addressed.

E-mail: lunjie@chalmers.se and eva.olsson@chalmers.se

Keywords: nanowires, electrical contacts, PN junction, *in situ* electron microscopy, ion beam

Supplementary material for this article is available online

Abstract

GaAs nanowires with built-in p–n junctions possess unique properties, making them suitable as basic components in a range of device applications, such as solar cells and photodetectors. Establishing reliable nanoscale electrical contacts on individual nanowires is crucial for characterizing and optimizing nanowire-device performances, but it is challenging due to the nanoscale material dimensions. Here, we show the optimization of electrical contacts on individual GaAs nanowires with built-in radial p–i–n junctions using site-specific nanoscale ion beam milling. We quantitatively studied the effect of ion beam treatment on the contact structure and properties using electrical characterization, theoretical modeling and transmission electron microscopy measurements. The electrical current rectifying effect at the electrode/nanowire contacts is diminished by the ion beam treatment, as evidenced by both dark and illuminated current–voltage (I–V) characteristics of the individual nanowires. The optimized nanoscale contacts allow the study of the intrinsic photovoltaic performance of the individual GaAs nanowires. Different from the conventional method of reducing rectifying contact by increasing semiconductor doping at the contacts, the contact improvement by ion beam processing is found to be mainly due to a decrease (up to 3 orders of magnitude) in the shunt resistance at the electrode/nanowire Schottky barrier. The combined electrical and structural measurements suggest that the shunt resistance change could be attributed to the modification of the microscopic structure at the contacts: the native oxide on the surface of the nanowires was removed by the ion milling; ion implantation creates a defect-rich surface layer on the nanowires at the contacts. The observations in this study provide new insights into the effect of ion beam processing on nanoscale electrical contacts and may contribute to the fabrication of reliable electrical contacts on not only nanoscale p–n junctions but also semiconducting nanostructures and devices in general.

1. Introduction

Semiconductor nanowires possess unique properties that are suitable for applications in a range of electronic and optoelectronic devices. In particular, III–V compound nanowires such as GaAs and InP, are well suited for photovoltaic and photodetection/emission devices due to their direct band gaps within the solar spectrum and high charge mobilities [1–4]. The vertical geometry of the nanowires enhances the absorption/emission of photons due to the waveguiding effect [5, 6]. The nanowire geometry also offers other advantages compared to thin film geometries, such as the growth of defect-free lattice mismatched heterostructures [7] and reduced material consumption due to efficient light trapping [8, 9]. Thus, III–V nanowires with built-in p–n junctions have shown promising photovoltaic performance and attracted significant research interest for applications in next-generation solar cells with high efficiency and low cost [2, 3, 10, 11]. One particularly promising geometry of the built-in junction is a radial p–i–n junction, where usually the p-doped core in the nanowires is directly grown on and thus electrically connected to a p-doped Si substrate, while the n-doped shell needs to be connected to electrical circuits via externally fabricated contacts [12–15]. The radial p–i–n junction provides an important advantage that the light-generated charge carriers are always near the junctions, enabling efficient charge separation and transportation.

The characterization of the performance of as-grown single p–i–n nanowires is of particular importance for the understanding and optimization of nanowire array-based devices [16, 17]. Though challenging, the study of the electrical and optoelectronic performance of individual nanowires with radial p–i–n junctions has previously been realized by both lithography techniques [5] and *in situ* electron microscopy (EM) methods [18, 19]. However, one significant challenge for realizing single-nanowire studies is the establishment of reliable local electrical contacts on the individual as-grown nanowires. In particular, the radial p–n junction geometry of the nanowires poses technical difficulty in fabricating high-quality contacts on the p- and n- layers, due to the nanoscale dimensions of the layers and the close vicinity of the contacts to the p–n junction.

Previously, reliable and high-quality electrical contacts have been successfully fabricated on assemblies of III–V nanowires with built-in p–n junctions on their as-grown substrates, using lithography procedures [3, 20]. Such contacts enabled the characterization and realization of III–V nanowire devices with record-high photovoltaic energy conversion efficiencies. Later on, it has also been demonstrated that it is possible to apply the standard lithography procedures to establish reliable electrical contacts on individual III–V p–i–n nanowires on growth substrates [5]. However, in this process, nanowires from a large area in the vicinity of the contacted nanowire on the growth substrates need to be removed or damaged, to avoid contacting multiple nanowires simultaneously [5]. Thus, the standard lithography and annealing procedures are not suited to fabricate electrical contacts on individual nanowires on their growth substrates, while avoiding destructing the as-grown nanowire assembly. In contrast, *in situ* nanoprobing EM is a highly versatile technique, since nanowires on the growth substrates can be characterized by contacting the nanowires individually using a movable metallic nanoprobe [18]. In this way, the electrical and photovoltaic properties of individual nanowires in nanowire assemblies on as-grown substrates can be selectively characterized, without affecting other nanowires in the assemblies. Single-nanowire measurements can be performed in sequence on multiple nanowires in the same assembly using the setup. Such measurements are valuable for assessing nanowire performance at the single-nanowire level, providing critical information about material quality, light–matter interaction, charge generation and separation at the nanometer scale. The information is of importance for the further development of semiconducting devices comprised of nanomaterials for solar energy harvesting and photodetection, as well as for establishing other important devices utilizing single nanomaterials. However, for measurements on single nanowires using a nanoprobing setup, the contact is usually made directly between the metal nanoprobe and the semiconductor nanowire. Though this procedure does not require the sophisticated lithography process or high temperature annealing [21, 22], the resulting contacts are often non-ideal, with high resistances and strong rectifying effects. Non-Ohmic and rectifying contacts have detrimental effects on the semiconductor device performance. For example, rectifying contacts significantly reduce photocurrent and strongly affect the illuminated I–V characteristics of solar cells and photodetectors [23]. Furthermore, non-linear contacts could hinder accurate characterization of the device's electrical properties.

In situ ion milling and Joule heating have been attempted in our previous work for optimizing the nanoscale contact on GaAs nanowires with built-in radial p–i–n junctions using an *in situ* nanoprobing setup [18, 19]. Both techniques have been shown to be capable of improving the contacts between a metal probe and the GaAs nanowires, though Joule heating is more difficult to control. The p–n junction could be modified by excessive electrical current used for Joule heating. In contrast, site-specific ion milling treatment of individual nanowires prior to contact metal deposition can be used to reproducibly minimize the rectifying effect at the contacts and even establish nanoscale Ohmic contacts [24–27]. Though effective, the impact of ion milling treatment on the nanowire structure and the mechanism of contact optimization are still not fully understood.

In this work, we demonstrate a technique involving ion beam treatment using a focused ion beam (FIB) to improve the electrical contacts on individual GaAs nanowires with built-in radial p–i–n junctions on a growth substrate. Using an in-house developed *in situ* EM nanoprobing setup, we studied and compared the electrical and photovoltaic properties of individual nanowires contacted either as-grown or after FIB milling. Detailed microstructures of the nanowires with and without ion milling at the contact interface were studied by transmission electron microscopy (TEM). Based on the experimental measurements and theoretical modeling, mechanisms of contact optimization via ion beam treatment are discussed.

2. Experimental

2.1. Nanowire growth

The GaAs nanowires were fabricated through self-catalyzed molecular beam epitaxy [5]. The nanowires were grown epitaxially on a p-doped (111) Si substrate with native oxide. The substrate was heated to 630 °C and a flux of Ga and As_4 was added into the chamber. The p-doping of the core was achieved by introducing a flux of Be during the axial growth of the nanowires. The intrinsic and n-doped shell of the nanowires were grown radially at 430 °C. The n-doping was achieved by introducing a flux of Si during the radial growth.

2.2. FIB instrumentation

A FEI Versa3D FIB—scanning electron microscope (FIB-SEM) was used for *in situ* ion beam processing for contact optimization on individual GaAs p–i–n nanowires, depositing contact metal on the nanowires, and manipulating and transferring individual nanowires. Detailed parameters used for contact optimization by ion beam treatment are presented in the results section. Moreover, *in situ* electrical and photovoltaic property measurements on individual nanowires were also carried out in the FIB-SEM using a custom-made nanoprobing setup. In addition, the FIB-SEM was used for cross-sectional TEM sample preparation of the contacts on the nanowires as well.

2.3. Scanning tunneling microscope—SEM (STM-SEM) nanoprobing setup for electrical and photovoltaic measurements

Electrical and photovoltaic measurements on individual GaAs p–i–n nanowires were enabled by a custom-made STM-SEM nanoprobing setup [18, 19]. A piezo-controlled STM probe made of Au was used to approach single nanowires to contact the n-doped shell of the nanowires. The p-doped core of the nanowires is directly connected to the p-Si substrate during nanowire growth. An electric circuit containing the nanowire p–i–n junction was formed by connecting the nanoprobe and the Si substrate to sense and source terminals of a Keithley 2450 SourceMeter, respectively. A light emission diode was also integrated in the STM-SEM setup, allowing the illumination of the nanowires with white light for photovoltaic measurements of individual nanowires.

2.4. TEM instrumentation

Selected area electron diffraction, bright field (BF) and dark field (DF) TEM imaging were performed in a FEI Tecnai T20 equipped with a LaB_6 electron source and operated at 200 kV. Scanning transmission electron microscopy—energy dispersive x-ray spectroscopy (STEM-EDS) measurements were performed in a JEOL monochromated ARM200F TEM with an electron beam energy of 200 kV. The microscope is equipped with a Schottky field emission gun, a double-Wien monochromator, a probe Cs aberration corrector, an image Cs aberration corrector, a double silicon drift detector for EDS, and a Gatan image filter Continuum.

3. Results

3.1. Effects of site-specific ion beam contact processing on electrical and photovoltaic properties of individual GaAs nanowires with radial p–i–n junctions

3.1.1. In situ fabrication and electrical characterization of contacts on individual as-grown GaAs p–i–n nanowires

Each nanowire was doped to form a core–shell p–i–n junction, with a p-doped (Be) core, an n-doped (Si) shell and a thin intrinsic layer in between. The diameter of the core is approximately 100–120 nm and the thicknesses of the intrinsic and n-doped layers are approximately 15 nm and 60–80 nm, respectively. To make electrical contact to individual as-grown nanowires on a Si substrate, we used a piezo-controlled nanoprobe setup inside a FIB—SEM [18]. The p-doped nanowire core was connected directly to the p-doped Si substrate. An STM Au probe was used to contact the n-doped nanowire shell. The Au nanoprobe was first brought into contact with the nanowire (figure 1(a)). At this stage, the electrical contact is highly resistive and rectifying. Moreover, the contact is unreliable since any mechanical instability will affect the interface between the nanowire and the probe. Electron beam induced Pt-deposition (EBID-Pt) in the FIB-SEM was used to attach the nanowire to the Au probe (figure 1(a)). In the EBID-Pt process, a Pt-containing gaseous organic precursor was decomposed by an electron beam (beam energy $\sim$ 5 kV, beam current $\sim$ 4 nA) at room temperature in the high vacuum chamber of the FIB-SEM, leading to the local deposition of Pt (together with amorphous carbon) in the area on

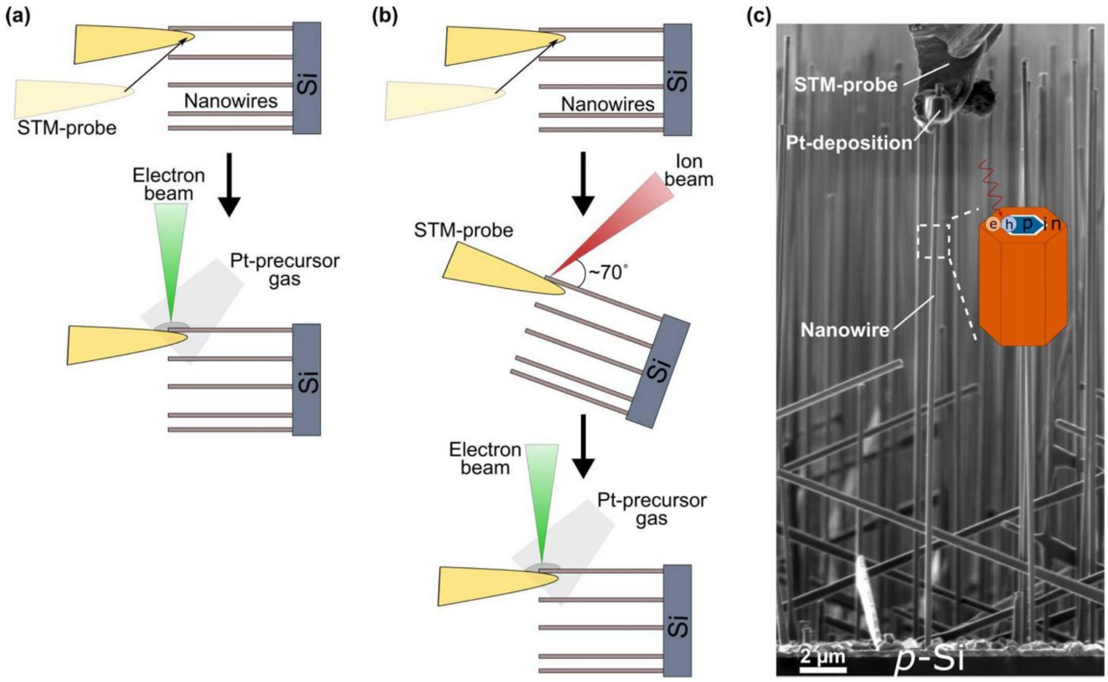

Figure 1. Establishing nanoscale electrical contacts to single GaAs nanowires with built-in p–i–n junctions on *p*-Si substrate in an *in situ* nanoprobing setup using a FIB-SEM. (a) Schematic illustration of the process for making electrical contacts to a single as-grown nanowire on the growth substrate (as-grown contact). Initially, the Au probe is brought into mechanical contact of the nanowire tip by piezo-controlled movement. Thereafter, electron beam induced deposition (EBID) of Pt is used to stabilize the probe-nanowire contact and increases the contact area. (b) Schematic illustration of the process for making improved electrical contact using ion milling. The probe is brought into mechanical contact with the nanowire from underneath, with respect to the electron beam source. Thereafter, the ion beam is scanned over the nanowire area where the Au probe and the nanowire are overlapping. Finally, EBID-Pt is used to make contact between the FIB-exposed area of the nanowire and the Au probe. (c) SEM image of a gold probe contacted to a single GaAs nanowire through the procedure depicted in (b). The inset shows a schematic of the p–i–n junction in the nanowire. Each nanowire contains a radial p–i–n junction, which enables the nanowires to be used as solar cells by separating and collecting electron–hole pairs generated by incident light.

the nanowire surface that was scanned by the electron beam. The decomposition process occurs mostly via low energy electron impact from secondary electrons and inelastically backscattered electrons generated from the nanowire surface. The EBID-Pt was chosen as the contact metal due to two main reasons. First, the electron beam-induced decomposition process is a relatively low energy process and does not affect the nanowire structure through effects such as implantation. Second, Pt is chemically stable, and the deposition process occurs at room temperature, preventing solid-state reaction between Pt and the nanowire. The interfacial structure between the EBID-Pt and the nanowires is presented in detail in section 3.3. The Pt-deposition also ensures that the contact is mechanically stable, allowing reliable and reproducible electrical measurements. Effectively, the electrical behavior of the nanoscale electrical contact on the nanowire is determined by the EBID-Pt/nanowire contact since the area of the nanowire/Au probe interface is much smaller. The contacts made in this way (as-grown contacts) still tend to be non-Ohmic and highly resistive. To further optimize the electrical contact, we adopted a procedure based on nanoscale FIB-milling (figure 1(b)). In this procedure, the first step is again to bring the Au STM probe into contact with the nanowire. This is followed by local FIB-milling of the top surface of the nanowire in the area where the probe and the nanowire overlap. A Ga^{+} ion beam with a beam energy of 2 kV and a beam current of 27 pA was used, and the tip of the nanowire was exposed to the ion beam for 10–20 s. The parameters for the FIB-milling were chosen to minimize potential beam damage to the p–i–n junction. Then, EBID-Pt was deposited at the ion milled surface region of the nanowire. As a result, the Au probe and the FIB-exposed tip of the nanowire were welded together by EBID-Pt. An example of a single GaAs nanowire contacted in this way is shown in the SEM image in figure 1(c). The contact area can be estimated by the extension of Pt-deposition along the nanowire (typically 1–3 μm) times the circumference of the nanowire, because the Pt-deposition generally covers the back side of the nanowire as well. To make sure that no other nanowires were contacted, the probe was moved sideways back and forth during live SEM imaging, to confirm that only the FIB-milled nanowire followed the motion of the probe.

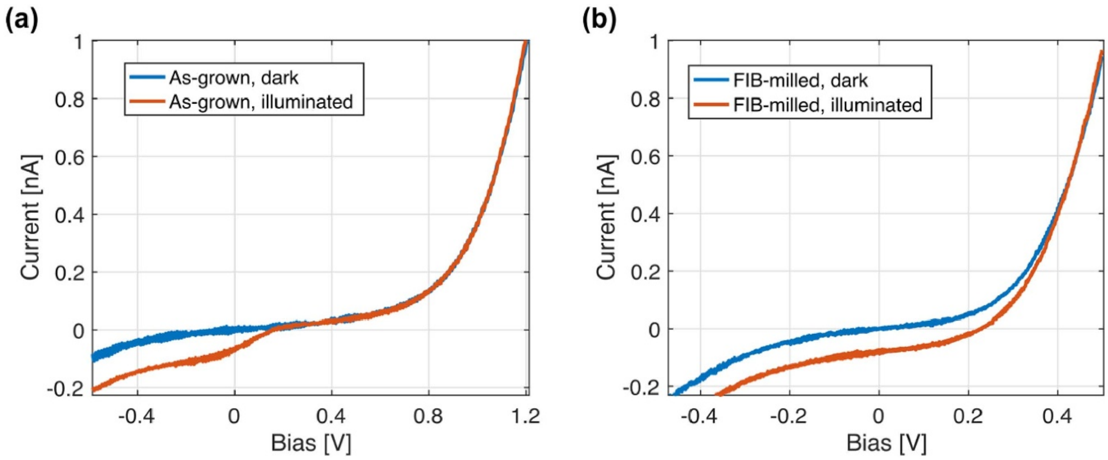

Figure 2. (a) Dark and illuminated I–V characteristics of a nanowire contacted as-grown. There is a clear S-shape around the zero-bias point in the illuminated I–V curve, showing a rectifying electrical contact behavior. (b) Dark and illuminated I–V characteristics of a nanowire with FIB-processed contact. The illuminated I–V curve has no S-shape.

To assess the quality of the electrical contacts we performed both dark and illuminated *I–V* measurements of several nanowires contacted either as-grown or after FIB-milling at the tip of the nanowires. Figure 2(a) shows the *I–V* characteristics of a representative nanowire that was contacted as-grown, i.e. without FIB-milling. The dark *I–V* characteristics show a non-linear, almost symmetric behavior within a low bias range (−1 V to 1 V). The relatively high current at reverse bias is most likely due to a leakage path between the n-doped shell and the p-doped Si substrate at the nanowire base. In a higher bias range (−4 V to 4 V), the *I–V* characteristics are rectifying, as expected from a p–n junction (see also Supporting information (SI) figure S1). In the illuminated *I–V* curve in figure 2(a), an anomalous S-shape around the zero-bias point was observed. The distinctive S-shaped *I–V* characteristics are attributed to a rectifying (Schottky) electrical contact connected in series to the p–n junction [23, 28], see SI figure S2 for more information. At negative bias, the illuminated *I–V* curve is shifted downwards with respect to the dark *I–V* curve due to the contribution of the photocurrent collected by the p–n junction. However, the photocurrent starts to diminish rapidly around zero bias and finally disappears at a relatively small positive bias (∼180 mV). The S-shape in *I–V* characteristics results in a dramatic loss in photovoltaic energy conversion efficiency and hinders a reliable assessment of the inherent nanowire properties. The nanowire contacted as-grown has a short circuit current (I_{SC}) of 73 pA, an open-circuit voltage (V_{OC}) of 174 mV and a fill factor (FF) of 0.23. Turning our attention to the *I–V* characteristics of a nanowire with a FIB-milled contact (figure 2(b)), the situation is quite different. Here, the illuminated *I–V* curve has no S-shape. Instead, it has almost the same shape as the dark *I–V* curve, indicating a non-rectifying contact. The I_{SC}, V_{OC} and FF for the FIB-milled nanowire are 80 pA, 226 mV and 0.44, respectively. As a result, the maximum output power is a factor 2.7 higher than for the nanowire contacted as-grown. In total, photovoltaic measurements were performed on 6 nanowires with as-grown contacts and 3 nanowires with FIB-milled contacts. Generally, the nanowires contacted by the FIB-milling procedure did not have S-shape *I–V* characteristics under illumination, resulting in higher FFs compared to the nanowires contacted as-grown (table 1 and figure S4). Furthermore, *I–V* measurements without illumination were performed on 12 nanowires with as-grown contacts and 5 nanowires with FIB-milled contacts. There was a clear trend that the FIB-milled nanowires had higher forward dark currents and lower ideality factors than the as-grown nanowires (table 2 and SI S3), indicating improved contacts.

3.1.2. Theoretical modeling of charge transport through the contacts and the nanowires

To better understand the effect of FIB-milling on the electrical behavior of the contacts, we used a theoretical model to simulate the charge transport through the contacts and the nanowires. In this model, the p–i–n junction within the nanowires and the Schottky junction at the contacts are represented by two diodes connected in series ‘head-to-head,’ see figure 3(a). An insulating barrier is included in the modeling of the Schottky diode to represent a native oxide layer on the nanowire surface, which has been commonly observed on GaAs [29] and is described in section 3.3. A current generator in parallel to the p–n diode represents the photocurrent generated during light illumination. A shunt resistance is added in parallel to each diode, representing a leakage current path through the barriers. Lastly, the

Table 1. Photovoltaic parameters, including short circuit current (I_{SC}), open circuit voltage (V_{OC}), and fill factor (FF), extracted from the *I–V* characteristics (figure S4) of 6 nanowires with as-grown contacts and 3 nanowires with FIB-milled contacts.

	I_{SC} (pA)	V_{OC} (mV)	FF
As-grown	43	173	0.23
As-grown	54	168	0.24
As-grown	86	272	0.22
As-grown	12	162	0.22
As-grown	76	228	0.23
As-grown	73	174	0.23
FIB-milled	80	226	0.44
FIB-milled	80	146	0.30
FIB-milled	53	86	0.28

Table 2. Ideality factors extracted from the dark *I–V* characteristics of 12 nanowires with as-grown contacts and 5 nanowires with FIB-milled contacts. The corresponding *I–V* curves are presented in figure S3.

	Ideality factor (n)											
As-grown	12.4	14.7	6.0	10.5	12.2	8.7	10.2	13.2	10.5	12.5	10.6	10.1
FIB-milled	6.9	3.7	5.8	4.3	4.9							

Table 3. Parameter values for *I–V* characteristics simulations. R_{Sh1} and R_{Sh2} are shunt resistances at the p–i–n junction and contact, respectively. R_S is the series resistance. I_{ph} is the photogenerated current and I_S is the diode saturation current of the p–i–n junction. ϕ_b is the barrier height of the Schottky barrier at the contact. ζ is the difference between the Fermi energy and the bottom of the conduction band at the Schottky junction. N_d is the doping concentration of the semiconductor. λ is the barrier height (in eV) of the insulating native oxide layer and δ is its thickness (in Å). n_1 and n_2 are the diode ideality factors for the p–i–n junction and the Schottky junction, respectively. S is the contact area.

	As-grown	FIB-milled	Ohmic
R_{Sh1}	12 GΩ	12 GΩ	12 GΩ
R_{Sh2}	100 GΩ	80 MΩ	—
R_S	2.0 MΩ	1.0 MΩ	1.0 MΩ
I_S	10 pA	7.0 pA	7.0 pA
I_{Ph}	100 pA	80 pA	80 pA
$\emptyset_b$	0.34 eV	0.42 eV	—
ζ	0.02 eV	0.02 eV	—
δ	35 Å	15 Å	—
N_d	$5.7{\cdot}10^{23}$ m^{-3}	$6{\cdot}10^{23}$ m^{-3}	—
n_1	3.5	3.5	3.5
n_2	1	1	—
λ	0.1 eV	0.1 eV	—
S	$3{\cdot}10^{-12}$ m^2	$3{\cdot}10^{-12}$ m^2	—

undepleted part of the nanowire is represented by a series resistance. More details about the theoretical model are provided in SI S4. The simulated *I–V* characteristics of a nanowire with Ohmic contact are obtained by excluding the Schottky diode and the associated shunt resistance from the circuit. The model was used to fit the experimental illuminated *I–V* characteristics of nanowires with contacts fabricated on as-grown nanowires or after FIB-milling (figures 3(b) and (c)). Table 3 shows the values of the different parameters used for the simulated *I–V* curves in figure 3. The contact area, *S*, and the thickness of the insulating layer, δ, are estimated from SEM and TEM images. The rest of the parameter values have been chosen to fit the experimental data.

The *I–V* curve of the nanowire with FIB-treated contact is very similar to the Ohmic *I–V* curve at low biases (figure 3(b)), but they are significantly different at high bias (figure 3(c)). According to the modeling, there are two main differences between the as-grown and the FIB-milled contacts. First, R_{Sh2} (the shunt resistance at the contact) decreases by approximately 3 orders of magnitude due to the FIB-milling. Such a low value of R_{Sh2} is the main reason that the FIB-milled contact shows close to Ohmic behavior at low biases, and the diminishment of the S-shape. Second, the width of the insulating barrier

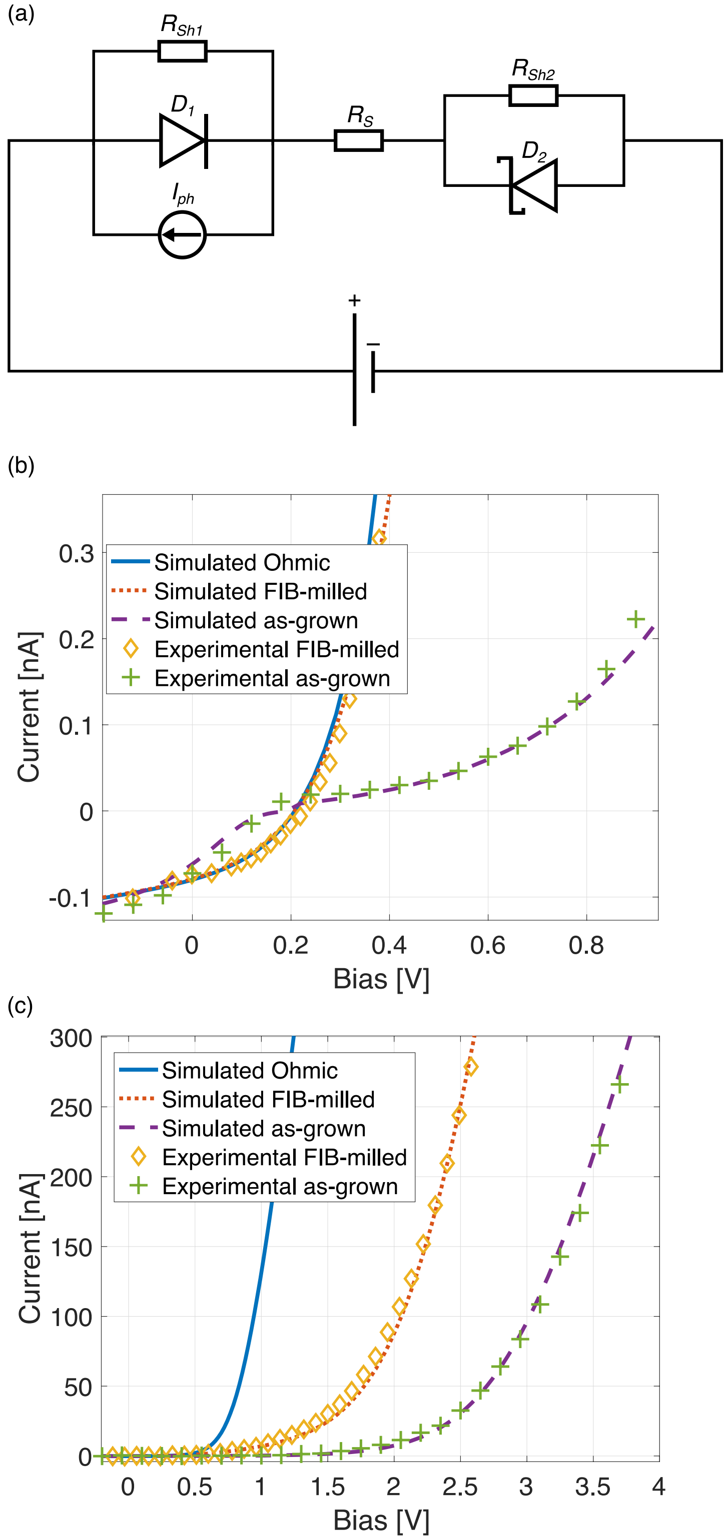

Figure 3. (a) Equivalent electrical circuit for the nanowire–contact system. (b) and (c) Modeled and experimental I–V characteristics for the as-grown and ion milled contacts at low and high bias ranges, respectively.

at the contact is reduced by the FIB-milling. This is the main reason for the increased current at high bias in the FIB-milled nanowire compared to the as-grown one.

3.2. Effects of ion beam processing on electrical contacts and charge transport through the n-doped shell

In order to study the electrical behavior of the contacts without the influence of the p–i–n junction, measurements were also performed on nanowires contacted only through the n-doped shell. Vertical

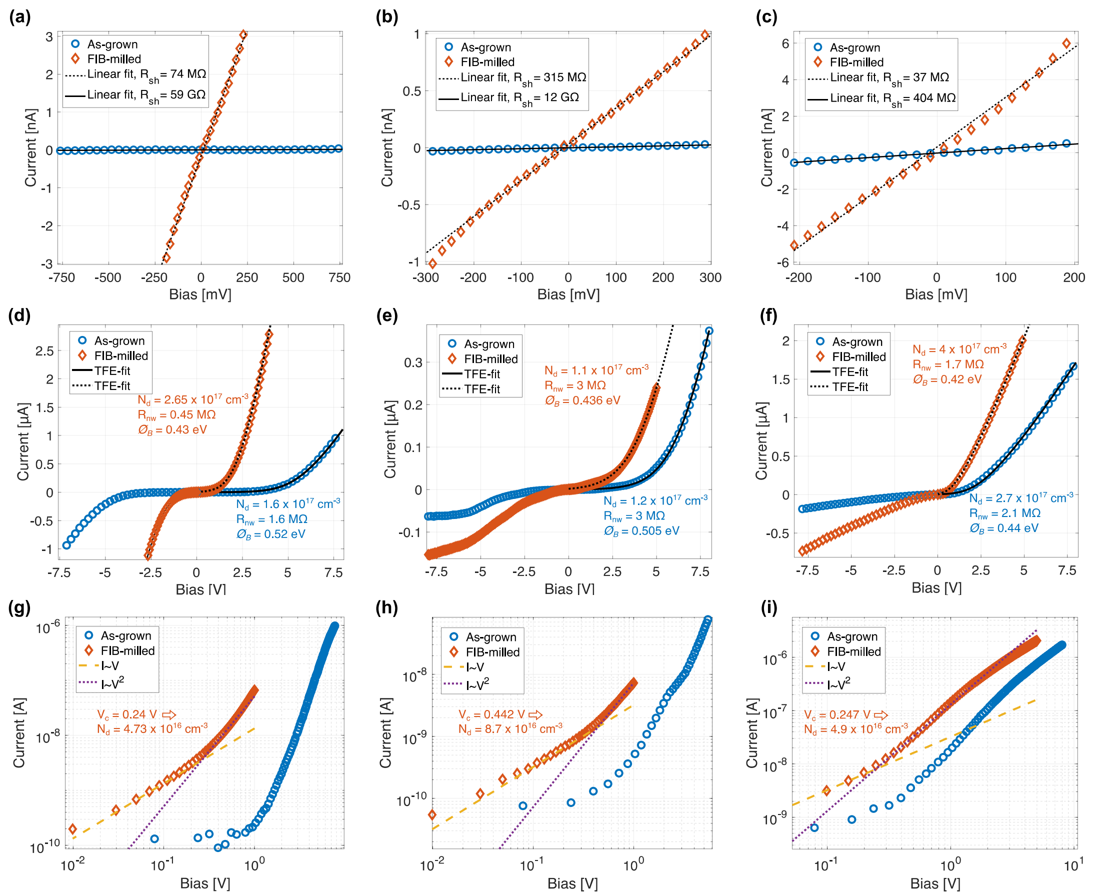

Figure 4. Dark I–V characteristics of the n-doped shell of horizontal nanowires contacted both as-grown and FIB-milled. Each column represents results from one nanowire. (a)–(c) Low bias regime I–V characteristics from the −200 to 200 mV range, showing the differences in R_{sh} between the two contact types. (d)–(f) High bias regime I–V characteristics with TFE fits. (g)–(i) I–V characteristics on a log–log scale with straight lines corresponding to I ∼ V and I ∼ V^2.

GaAs nanowires with p–i–n junctions on growth substrates were mechanically broken at the base by scratching the growth substrate with a scalpel. Subsequently, individual nanowires lying horizontally on the growth substrate were picked up by an OmniProbe (Oxford Instruments) micromanipulator in the FIB-SEM and transferred to a separate Si substrate with a 400 nm thick SiO_2 surface layer and pre-patterned Au electrodes, see figure S5. After that, two contacts were made on the n-doped shell of the nanowire and connected to the Au electrodes by EBID-Pt, forming as-grown contacts. Two FIB-processed contacts were formed on the same nanowire by first irradiating two sub-micrometer scale areas on the nanowire between the as-grown contacts with a focused Ga^+ ion beam in the FIB-SEM. The parameters for ion beam irradiation are the same as those shown in section 3.1 (acceleration voltage 2 kV, beam current 27 pA, milling time 10–20 s, see figure S5). After ion beam irradiation, contacts were made on the milled areas of the nanowire and connected to the Au electrodes by EBID-Pt. Electrical characterization of both the as-grown and the FIB-processed contacts on the same nanowire was carried out. In total, 3 nanowires were characterized in the way described above, and the results are shown in figure 4. Each column in figure 4 shows results from one nanowire. In the first row (figures 4(a)–(c)), I–V characteristics of as-grown contacts and FIB-milled contacts in the low bias range are shown. The FIB-milled contacts have shunt resistances (R_{sh}) that are 1–3 orders of magnitude lower than the as-grown contacts, extracted from the linear I–V regime from −200 to 200 mV. The second row (figures 4(d)–(f)) shows I–V characteristics in a higher bias range. The thermionic field emission (TFE) model (see SI S4) was used to fit the positive side of the I–V curves and extract three parameters: doping concentration (N_d), nanowire resistance (R_{nw}) and effective Schottky barrier height (ϕ_B). The FIB-milled contacts have a ϕ_B that is 0.02–0.09 eV lower than the as-grown contacts. Furthermore, R_{nw} is generally lower for the FIB-milled contacts, which could be explained by the fact that the distance between the FIB-milled contacts is always smaller than that between the as-grown contacts. According to the TFE-fitting, the doping concentrations of both the as-grown contacts and the FIB-milled contacts are

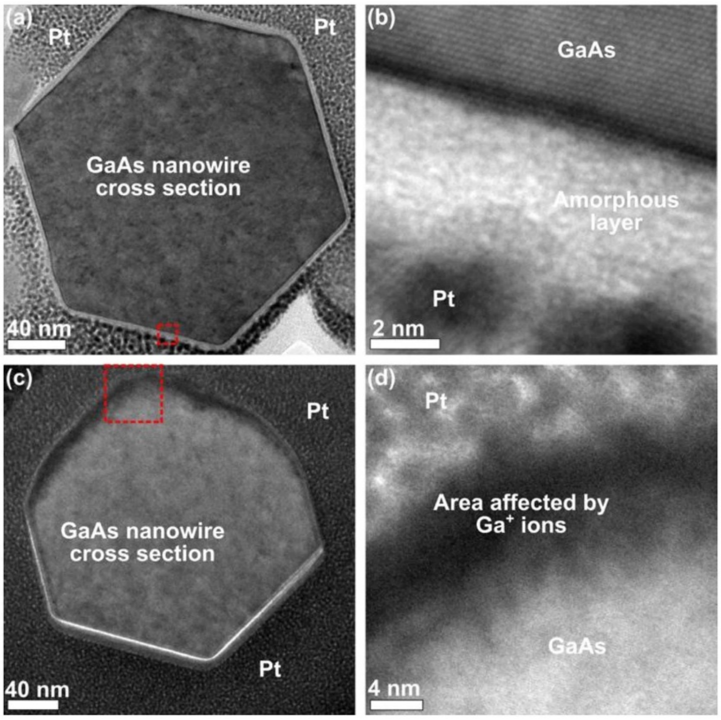

Figure 5. (a) TEM BF micrograph of a cross-section of a nanowire contacted as-grown. (b) High-resolution TEM micrograph of the area marked by the red square in (b). The crystalline GaAs and the Pt nanoparticles are separated by an amorphous layer which is around 4 nm thick. (c) TEM BF micrograph of a cross-section of a FIB-milled nanowire. (d) High-resolution TEM image of the area marked by the red square in (c). The EBID Pt is in direct contact with the area that was affected by the FIB-milling.

rather similar, around 1–4 × 10^{17} cm^{-3}. The TFE analysis is valid if the current is limited by the contacts. However, it is possible that the current is space-charge limited rather than limited by the contacts because of the small dimensions of the nanowires. Space-charge limited current (SCLC) results in I–V characteristics with $I \sim V^2$ and has been observed in semiconducting nanowires [30, 31]. To examine such a relationship in the GaAs nanowires, the I–V characteristics of the three nanowires are plotted on a log-log scale (figures 4(g)–(i)). The FIB-milled nanowires show quadratic I–V characteristics for an extended bias range, indicating SCLC. In this scenario, the doping concentration needs to be extracted as $N_d = \varepsilon V_c / qR^2$ with V_c being the crossover voltage where the current goes from Ohmic behavior ($I \sim V$) to SCLC behavior [30]. R is the nanowire radius and ε and q is the permittivity of the semiconductor and the elementary charge, respectively. According to this analysis, the doping concentrations at the FIB-milled contacts are around 4–8 × 10^{16} cm^{-3}. In contrast, for the as-grown contacts, the I–V characteristics do not have a clear quadratic dependency. The current is therefore limited by the contacts, and the TFE model should give the most accurate estimation of the doping concentration, which is about 1–3 × 10^{17} cm^{-3}.

3.3. Microstructure characterization of the contacts

To understand the underlying reason for the difference in electrical behavior between the two different types of contacts, we studied the microscopic structure of the two types of contacts using TEM. TEM BF images of the cross-section of a nanowire that was contacted as-grown are shown in figures 5(a) and (b). The nanowire cross section has a regular hexagonal shape. There is a 4–5 nm thick surface layer covering all the 6 facets of the nanowire (figure 5(b)). This surface layer is amorphous, as evidenced by the random image contrast in the TEM BF images, as well as electron diffraction and DF images (see figure S6). The interior of the GaAs nanowire has a single crystalline Zinc Blende structure. The EBID-Pt layer is clearly separated by the amorphous surface layer from the crystalline GaAs nanowire structure at the contact, indicating the absence of interdiffusion or intermixing between Pt and the nanowire structure in the EBID process. Cross-sectional TEM images of a contact fabricated after ion beam treatment are shown in figures 5(c) and (d). The FIB-milling modified the material structure on the nanowire surface. In the ion milled area, the nanoscale amorphous surface layer was milled away. Moreover, the nanowire surface structure was modified by the Ga^+-ions, indicated by a darker contrast in the ion milled area in the TEM BF image and the change in nanowire morphology (figure 5(d)). The nanowire area at

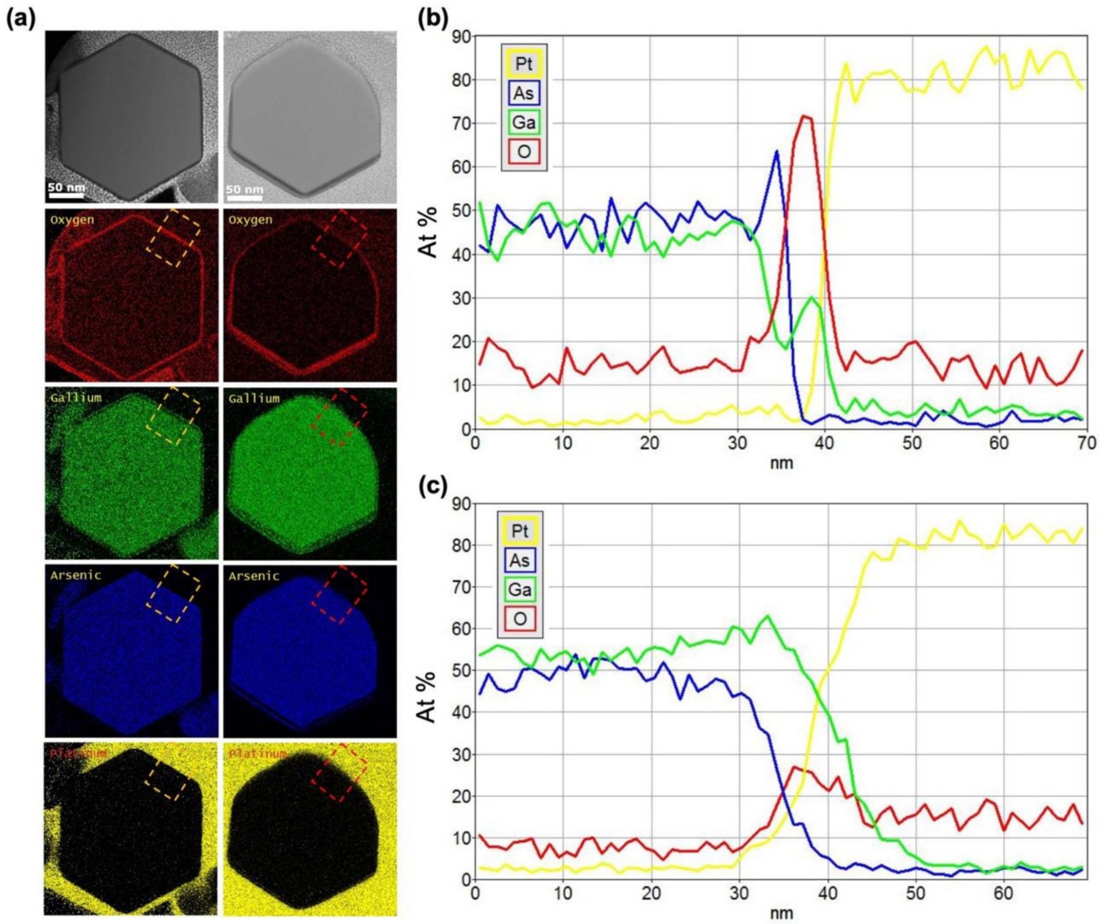

Figure 6. Elemental analysis of the as-grown and FIB-milled contacts. (a) HAADF STEM micrograph and elemental EDS-maps of as-grown (left column) and FIB-milled (right column) contacts. There is a strong oxygen signal at all facets of the as-grown nanowire. In the FIB-milled nanowire, the oxygen signal is weaker at the upper-right facets, which have been exposed to the ion beam. (b) Averaged EDS profile of the dashed rectangle in the left column in (a). Inside the nanowire the concentration of Ga and As are similar. Towards the nanowire edge there is first a slight increase in As and a decrease in Ga concentration, followed by a layer with only Ga and O. This is the native oxide layer covering the nanowire surface. The Pt is not directly in contact with the GaAs. (c) Averaged EDS profile of the dashed rectangle in the right column in (a). The Ga and As concentrations are similar inside the nanowire. However, approaching the edge of the nanowire the Ga concentration increases relative to the As.

the contact with the darker contrast has amorphous structure, as evidenced by TEM DF imaging (see figure S6). The crystal structure of the interior of the nanowire is still intact. By comparing the FIB-milled nanowire cross section with a regular hexagon, we estimate that only the outermost 10–30 nm of the nanowire is milled away or affected by the ion beam. From a nanowire geometry point of view, the p–i–n junction at the contact is still present after FIB-milling, since the n-doped layer is 60–80 nm thick. Electrical measurements (e.g. I–V characteristics shown in section 3.1) also show that the p–i–n junction at the ion-milled region is not short-circuited, as evidenced by the rectifying behavior and sizable photocurrent in the I–V measurements. This is in contrast to the expected linear I–V characteristics and a diminished photovoltaic effect of short-circuited p–i–n junctions. In addition, it is worth noting that the ion beam treatment is site-specific and performed in a relatively small section ($\sim$ 1 μm long) of a nanowire ($\sim$ 15–20 μm long). In the nanowire areas away from the tip region, the nanowire was not exposed to the ion beam, and the p–i–n junction was not affected.

STEM-EDS was performed to further investigate the effect of the FIB-milling on the material structure and composition at the contacts. Cross-sectional STEM annular dark field (ADF) images and corresponding elemental maps of O, Ga, As, and Pt of the two contacts are shown in figure 6. Similar as the TEM BF images, the STEM ADF images show that ion milling removed a thin layer of material on the surface, including the amorphous surface layer (figure 6(a)). The morphology of two facets on the nanowire surface is modified. In addition, there is a surface area with brighter image contrast than the interior of the GaAs nanowires for the contact treated by ion milling. The contrast variation at the contact indicates that the ion milling process modified material composition on the nanowire surface. STEM-EDS elemental maps of the nanowire contact without ion milling clearly shows that the amorphous surface layer observed in TEM and STEM imaging consists of predominantly Ga and O (the left column of figure 6(a)). This surface layer is therefore the native oxide layer, which is continuous and covers the outer surface of the nanowire, separating the GaAs nanowire and the EBID-Pt. The intactness of the native oxide layer of the nanowire at the contact confirms that there is no obvious intermixing or interdiffusion between Pt and nanowire structure caused by the EBID-Pt process. At the FIB-treated contact, the change in nanowire morphology is evident in the Ga and As elemental maps. Moreover, the O signal is diminished in the surface area where the ion beam milled the nanowire (the right column of figure 6(a)).

The EDS composition profiles in figures 6(b) and (c) provide detailed information about the elemental composition across the nanowire-Pt interface for the as-grown (figure 6(b)) and FIB-milled contacts (figure 6(c)). In the interior of the nanowires, away from the contacts, there is roughly the same amount of Ga and As. At the contact interfaces, the elemental composition of the as-grown and FIB-milled contacts differ significantly. In the as-grown contact, there is a peak in As concentration and a dip in Ga concentration close to the nanowire surface. This is likely due to an outward migration of Ga atoms when the insulating native oxide was formed. The surface native oxide layer consists of around 70 at % O and 30 at % Ga, and almost no As. In the FIB-milled nanowire, the O signal at the contact is largely diminished, decreasing to about 20 at %. The Ga concentration gradually increases towards the outer surface of the nanowire in the ion milled area. Such an increase in Ga concentration is attributed to Ga^+-ion implantation during ion beam treatment. At the contact interface, the nanowire consists mostly of Ga. In addition, there is a slight increase in Pt EDS signal at the contact interface, within a layer with a thickness of $\sim$5 nm. This change in Pt signal is likely due to an increase in surface roughness of the nanowire (evident in TEM and STEM images) caused by ion milling before EBID of Pt, as implantation and interdiffusion are not expected in the EBID-Pt process. The modification of the material structure at the nanowire contacts provides important insights into the mechanism of the observed contact optimization by site-specific ion milling treatment at the nanometer scale.

4. Discussion

The direct correlation between the quantitative electrical characterization and structural measurements provides unique insights into the material mechanism of contact improvement by site-specific FIB treatment. The TEM analysis shows that there is no obvious interfacial intermixing or interdiffusion between the EBID-Pt and the nanowires (including the native oxide). This is consistent with the fact that EBID-Pt is a deposition process induced by low energy electrons at room temperature. Though the quality (such as resistivity and work function) of the EBID-Pt could be modified by the experimental conditions used for deposition and affect the contact characteristics, the same electron beam and deposition parameters were used for the EBID-Pt in this study. As a result, the quality of the EBID-Pt is not expected to vary between samples in the experiments. The changes in contact characteristics are thus believed to mainly originate from the modifications of the nanowire structure at the contact area induced by ion beam processing. The removal of the native oxide layer on the nanowire narrows the potential barrier at the metal-semiconductor junction, increasing the tunneling probability of charge carriers through the barrier. This leads to an overall higher current to pass through the contact. The distinctive S-shape in illuminated *I–V* curves of the p–i–n nanowires arises due to the rectifying character of the contact, which is a consequence of band-bending at the metal-semiconductor interface (see SI S2 and S4). It is the introduction of new conducting channels through the barrier (a reduction in shunt resistance) that is responsible for the diminishment of the S-shape, as shown by the modeling of the *I–V* characteristics (figure 3). Such a mechanism of contact optimization is markedly different from the commonly used method. Conventionally, the contact optimization is achieved by heavy doping of the semiconductor surface or metal diffusion and alloying in the semiconductor at the contact [32], resulting in a reduction in the Schottky barrier width/height [33]. Based on the electrical measurement on the n-doped shell of the nanowires (figure 4), the doping concentration is actually reduced after FIB-milling, which is in line with previous studies on ion milling effects [22, 34]. The contact-improvement is therefore not expected to be due to the change in doping concentration in the semiconductor. Instead, we demonstrate that the reduction in shunt resistance through ion beam processing plays a dominant role in realizing almost non-rectifying contacts on the GaAs nanowires. The TEM and STEM EDS data show that the ion milling results in Ga-implantation and amorphization of the nanowire surface, which may introduce electrically active defects at the interface between the Pt and the n-doped shell of the GaAs nanowires [34]. These localized electronic states could be the physical origin of the drastic reduction of the shunt resistance at the contact [35]. It is worth noting that the FIB-procedure we established, by carefully choosing ion beam energy, beam current as well as ion milling time and area, is site-specific, of high (nanometer scale) resolution, and deterministic. This procedure was controlled to selectively modify the n-doped shell at the contact region in the p–i–n nanowires, without short-circuiting the nanoscale p–n junction close to the contact. The defects created in the n-doped shell could increase carrier recombination, which may locally reduce electron mobility and negatively affect electron–hole pair separation. However, such an effect is expected to be insignificant. It is because the area exposed to Ga^+ ion beam treatment was subsequently covered by EBID-Pt to form the electrical contact on the n-doped shell. The EBID-Pt is not transparent to light, so the contribution of this area to electron–hole pair generation is negligible. Moreover, nanowire area treated by the Ga^+ ion beam is a small section ($\sim$1 μm long) of the nanowire ($\sim$15–20 μm long). The contribution of this area to charge transportation is relatively small. The negative impact of local defect generation by the ion beam is thus believed to be insignificant. EBID-Pt was used as the contact metal on GaAs nanowires, but the protocol used in this study is likely applicable to contacts formed between other metals and III–V nanowires since the contact improvement mainly originates from structure modification of the semiconductor by ion beam processing. The method and mechanism could also be applicable to nanostructures of other inorganic semiconductors, such as group IV and II–VI semiconductors, as the removal of native oxide and generation of electrically active defects in these materials could also be introduced by controlled ion beam processing [25, 36]. FIB-SEM with Ga^+ ion source is a commonly available instrument in device fabrication and material characterization labs. Thus, the ion beam processing method is an effective alternative for optimizing electrical contacts on semiconducting nanostructures when the conventional lithography, chemical etching (SI S7) and high temperature annealing techniques are not applicable.

5. Conclusion

In summary, we have investigated a method for making reliable nanoscale electrical contacts on individual GaAs nanowires with built-in radial p–i–n junctions on growth substrates, using *in situ* and analytical EM. The method utilizes site-specific FIB-milling of the nanowire surface followed by metal deposition. Electrical and photovoltaic properties of individual nanowires were characterized using a nanoprobing setup to reveal the effects of contact optimization by the ion beam processing method. TEM and STEM-EDS were used to study the effects of ion beam treatment on the microscopic structure at the nanoscale contact interfaces. The as-grown contacts show strong rectifying effect as being clearly manifested by distinctive S-shape characteristics in white light illuminated I–V curves, which significantly limit the photovoltaic performance of the nanowires. Ion beam treatment produces contacts with close to Ohmic behavior at low bias, and overall, less resistive. By correlating electrical measurements, theoretical model fitting and TEM analysis, the contact improvement by ion beam processing is attributed to two effects: the removal of the native oxide layer at the nanowire surface and the introduction of structural defects at the metal-semiconductor interface. The modification of surface structure of the semiconductor nanowire at the contact interface possibly gives rise to the significant ($\sim$3 orders of magnitude) reduction in shunt resistance at the contact. The shunt resistance reduction effectively diminishes the rectifying effect at the metal/semiconductor contacts and allows the establishment of contacts with close to Ohmic characteristics. The possible mechanism of contact optimization by ion beam processing found in this study is markedly different from that of conventional approaches, where contact improvement is caused by a reduction of the Schottky barrier height via heavy doping of the semiconductor at the contact. The present study contributes to fabricating high quality nanoscale contacts on semiconducting structures and devices.

Acknowledgment

J.H., L.J.Z., and E.O. acknowledge the financial support from Swedish Research Council (VR) under grants no. 2016-04618 and no. 2020-05432, Excellence Initiative Nano at Chalmers University of Technology, as well as the Knut and Alice Wallenberg Foundation (2019.0140). This work was performed in part at the Chalmers Material Analysis Laboratory, CMAL.

Data availability statement

All data that support the findings of this study are included within the article (and any supplementary files).

Conflict of interest

The authors declare no competing financial interest.

ORCID iDs

Jonatan Holmér 0000-0002-4213-5494
Lunjie Zeng 0000-0002-4564-7217
Eva Olsson 0000-0002-3791-9569

References

[1] Barrigón E, Heurlin M, Bi Z, Monemar B and Samuelson L 2019 Synthesis and applications of III–V nanowires *Chem. Rev.* **119** 9170–220
[2] Hrachowina L, Zhang Y, Saxena A, Siefer G, Barrigon E and Borgström M T 2021 Development and characterization of a bottom-up InP nanowire solar cell with 16.7% efficiency *2020 47th IEEE Photovoltaic Specialists Conf. (PVSC)* (IEEE) pp 1754–6
[3] Aberg I *et al* 2016 A GaAs nanowire array solar cell with 15.3% efficiency at 1 Sun *IEEE J. Photovolt.* **6** 185–90
[4] Prete P and Lovergine N 2025 High efficiency III–V nanowire solar cells: the road ahead *Nano Futures* **9** 042502
[5] Krogstrup P, Jørgensen H I, Heiss M, Demichel O, Holm J V, Aagesen M, Nygard J and Fontcuberta I Morral A 2013 Single-nanowire solar cells beyond the Shockley–Queisser limit *Nat. Photon.* **7** 306–10
[6] Yang P 2023 Semiconductor nanowire, what's next II? *Next Mater.* **1** 100014
[7] Makode P A, Muduli S P and Kale P 2025 A perspective of GaAs//Si Tandem photovoltaic cell: architecture, fabrication, and performance *Mater. Res. Bull.* **190** 113504
[8] Wen L, Zhao Z, Li X, Shen Y, Guo H and Wang Y 2011 Theoretical analysis and modeling of light trapping in high efficicency GaAs Nanowire array solar cells *Appl. Phys. Lett.* **99** 14
[9] Kuang Y, Vece M D, Rath J K, Dijk L V and Schropp R E I 2013 Elongated nanostructures for radial junction solar cells *Rep. Prog. Phys.* **76** 106502
[10] Otnes G and Borgström M T 2017 Towards high efficiency nanowire solar cells *Nano Today* **12** 31–45
[11] Van Dam D, Van Hoof N J J, Cui Y, Van Veldhoven P J, Bakkers E P A M, Gómez Rivas J and Haverkort J E M 2016 High-efficiency nanowire solar cells with omnidirectionally enhanced absorption due to self-aligned indium-tin-oxide Mie Scatterers *ACS Nano* **10** 11414–9
[12] Colombo C, Heiß M, Grätzel M and Fontcuberta I Morral A 2009 Gallium arsenide P-i-n radial structures for photovoltaic applications *Appl. Phys. Lett.* **94** 173108
[13] Mariani G, Scofield A C, Hung C-H and Huffaker D L 2013 GaAs nanopillar-array solar cells employing in situ surface passivation *Nat. Commun.* **4** 1497
[14] Mariani G, Zhou Z, Scofield A and Huffaker D L 2013 Direct-bandgap epitaxial core-multishell nanopillar photovoltaics featuring subwavelength optical concentrators *Nano Lett.* **13** 1632–7
[15] Boulanger J P, Chia A C E, Wood B, Yazdi S, Kasama T, Aagesen M and LaPierre R R 2016 Characterization of a Ga-assisted GaAs nanowire array solar cell on Si substrate *IEEE J. Photovolt.* **6** 661–7
[16] Li Z, Tan H H, Jagadish C and Fu L 2018 III–V semiconductor single nanowire solar cells: a review *Adv. Mater. Technol.* **3** 1800005
[17] Otnes G, Barrigo E, Sundvall C, Svensson K E, Heurlin M, Siefer G, Samuelson L, Åberg I and Borgstro M T 2018 Understanding InP nanowire array solar cell performance by nanoprobe-enabled single nanowire measurements *Nano Lett.* **18** 3038–46
[18] Holmér J, Zeng L, Kanne T, Krogstrup P, Nygård J, de Knoop L and Olsson E 2018 An STM—SEM setup for characterizing photon and electron induced effects in single photovoltaic nanowires *Nano Energy* **53** 175–81
[19] Holmér J, Zeng L, Kanne T, Krogstrup P, Nygård J and Olsson E 2021 Enhancing the NIR photocurrent in single GaAs nanowires with radial P-i-n junctions by uniaxial strain *Nano Lett.* **21** 9038–43
[20] Wallentin J *et al* 2013 InP nanowire array solar cells achieving 13.8% efficiency by exceeding the ray optics limit *Science* **339** 1057–60
[21] Timm R, Persson O, Engberg D L J, Fian A, Webb J L, Wallentin J, Jönsson A, Borgström M T, Samuelson L and Mikkelsen A 2013 Current-voltage characterization of individual as-grown nanowires using a scanning tunneling microscope *Nano Lett.* **13** 5182–9
[22] Suyatin D B *et al* 2014 Strong Schottky barrier reduction at Au-catalyst/GaAs-nanowire interfaces by electric dipole formation and fermi-level unpinning *Nat. Commun.* **5** 3221
[23] Zekry Z and Eldallal G 1988 Effect of MS contact on the electrical behaviour of solar cells *Solid State Electron.* **31** 91–97
[24] He J H, Chang P H, Chen C Y and Tsai K T 2009 Electrical and optoelectronic characterization of a ZnO nanowire contacted by focused-ion-beam-deposited Pt *Nanotechnology* **20** 13
[25] Ke J J, Tsai K T, Dai Y A and He J H 2012 Contact transport of focused ion beam-deposited Pt to Si nanowires: from measurement to understanding *Appl. Phys. Lett.* **100** 5
[26] Tham D, Nam C Y and Fischer J E 2006 Microstructure and composition of focused-ion-beam-deposited Pt contacts to GaN nanowires *Adv. Mater.* **18** 290–4
[27] Chen G, Gallo E M, Burger J, Nabet B, Cola A, Prete P, Lovergine N and Spanier J E 2010 On direct-writing methods for electrically contacting GaAs and Ge nanowire devices *Appl. Phys. Lett.* **96** 22
[28] Saive R 2019 S-shaped current-voltage characteristics in solar cells: a review *IEEE J. Photovolt.* **9** 1477–84

[29] Hollinger G, Skheyta-Kabbani R and Gendry M 1994 Oxides on GaAs and InAs surfaces: an x-ray-photoelectron-spectroscopy study of reference compounds and thin oxide layers *Phys. Rev. B* **49** 11159

[30] Talin A A, Léonard F, Swartzentruber B S, Wang X and Hersee S D 2008 Unusually strong space-charge-limited current in thin wires *Phys. Rev. Lett.* **101** 1–4

[31] Alagha S, Shik A, Ruda H E, Saveliev I, Kavanagh K L and Watkins S P 2017 Space-charge-limited current in nanowires *J. Appl. Phys.* **121** 17

[32] Rideout V L 1975 A review of the theory and technology for Ohmic contacts to Group III–V compound semiconductors *Solid State Electron.* **18** 541–50

[33] Piotrowska A 1993 Ohmic contacts to GaAs: fundamentals and practice *Acta Phys. Pol. A* **84** 491–504

[34] Brown S J, Rose P D, Jones G A C, Linfield E H and Ritchie D A 1999 Electrically active defect centers induced by Ga+ focused ion beam irradiation of GaAs(100) *Appl. Phys. Lett.* **74** 576–8

[35] Chattopadhyay P 1996 The effect of shunt resistance on the electrical characteristics of Schottky barrier diodes *J. Phys. D: Appl. Phys.* **29** 823–9

[36] Huang J, Loeffler M, Muehle U, Moeller W, Mulders J J L, Kwakman L F T, Van Dorp W F and Zschech E 2018 Si amorphization by focused ion beam milling: point defect model with dynamic BCA simulation and experimental validation *Ultramicroscopy* **184** 52–56